PNAS

Supporting Information for

Tree rings reveal the transient risk of extinction hidden inside climate envelope forecasts

Margaret E. K. Evans*[1†], Sharmila M. N. Dey[2†], Kelly A. Heilman[1†], John R. Tipton[3], R. Justin DeRose[4], Stefan Klesse[5], Emily L. Schultz[6], John D. Shaw[7]

[1] Laboratory of Tree-Ring Research, University of Arizona, Tucson, Arizona, USA 85721.
[2] Department of Earth and Planetary Sciences, Harvard University, Cambridge, Massachusetts, USA 02138.
[3] Statistical Sciences Group, Los Alamos National Laboratory, Los Alamos, New Mexico, USA 87545.
[4] Department of Wildland Resources and Ecology Center, Utah State University, Logan, Utah, USA 84322.
[5] Forest Dynamics, Swiss Federal Institute for Forest, Snow, and Landscape Research WSL, 8903 Birmensdorf, Switzerland.
[6] Department of Biology, Colorado Mountain College, Breckenridge, CO, USA 80424.
[7] Riverdale Forestry Sciences Lab, Rocky Mountain Research Station, USDA Forest Service, Riverdale, Utah, USA 84405.

† These authors contributed equally to this work

Corresponding author: Margaret Evans
Email: mekevans@arizona.edu

This PDF file includes:

Supporting text
Figures S1 to S13
Tables S1 to S3
SI References

Supporting Information Text

Biodiversity Forecasting with Occurrence Data

Predicting the impact of climate change on biodiversity has been dominated for the last twenty years by an approach that associates a species' occurrence (either presence-absence or presence-only data) with climate at those locations. The principle is illustrated in Fig. S1 with respect to a single temperature variable. In practice, this statistical model, known as a *species distribution model (SDM)*, *climate envelope model*, or *ecological niche model*, is created using many climate (or other predictor) variables at once. Excellent reviews of the methods are found in (1–3). The statistical model is then used to predict or forecast change in the species' geographic distribution with changing climate. In the single-variable example of temperature, with warming, the species' probability or rate of occurrence is predicted to increase at relatively cool locations (the *leading edge*) and decline at warmer locations (the *trailing edge*; Fig. S1B).

Climate responses across scales

In order for climate envelope or SDM predictions of range dynamics to actually come to pass, lower-level demographic variables, such as population size or density (abundance), population-level growth rate, or the net effect of individual-level vital rates (including growth, survival, and birth rates) should respond similarly to changing climate, either matching the entire response, including breadth (solid lines, Fig. S2), or, if more limited in breadth, they should reflect the local slope of the species-scale climate response curve (dashed lines, Fig. S2). Ecological theory supports this assumption: the *center-periphery hypothesis* predicts that individual-level performance and population-level growth rate decline from the center to the edge of a species' geographic and environmental distribution (Fig. S2). Under the *abundant-center hypothesis* and *Whittaker's continuum concept*, it is expected that a species' abundance is greatest at the center of its ecological niche (*i.e.*, climatic tolerances; Fig. S2). Though we note – these theoretical expectations concern time-averaged responses to spatial variation in climate (not responses to time-varying climate). Further, range dynamics in the real world are complicated by the lack of correspondence between position in geographic and environmental space – climatically average (or extreme) conditions are found throughout species' geographic distributions (4–6).

Climate response curves at different biological scales (individual, population, and species) and in response to spatial vs. temporal climate variation are influenced by a variety of different ecological processes. Further, they can take on a variety of shapes beyond a Gaussian, bell-shaped curve (unimodal, symmetric; Fig. S10A).

Individual Scale. Focusing on the scale of an individual organism, the phenotypic response of a single genotype to different environmental conditions is termed by population geneticists its *reaction norm*. A time series of an individual's growth rate is an example of a single genotype expressing different phenotypes (growth rates) when exposed to different conditions (interannual climate variation and any other differences between years). This interannual variation in growth is the result of *phenotypic plasticity*. *Thermal performance curves*, plastic responses to different temperature conditions, have been the subject of heightened interest in the context of anthropogenic warming (7). They are understood to be bounded at both a minimum and maximum value – organismal functionality goes to zero below a minimum temperature and above a maximum temperature (the *critical thermal maximum*). Between the minimum and maximum lies an optimum – a temperature at which individual-level physiological functioning reaches its peak. This thermal response curve may be symmetric (Gaussian) or left- or right-skewed (Fig. S10A). If skewed, the response may be approximated by a linear function across much of the range of temperatures to which the organism is regularly exposed and hence adapted (Fig. S10B). Other climate response curves at the individual scale may be saturating. For example, performance in plants may be a saturating function of soil moisture – increasing to a plateau, above which additional soil moisture leads to neither increased nor decreased performance (Fig. S10A).

Population scale. Climate response curves at the population scale, involving population size, density, or growth rate as responses, emerge as the net result of five demographic processes or *vital rates*: birth, death, immigration, emigration, and (in structured populations) changes in age, size, or developmental stage. Different vital rates may be affected by climate differently, even in an opposite manner – known as *demographic compensation*. The net effect of a climate variable on population growth rate is a function of its effect on each vital rate and the sensitivity of population growth rate to changes in each vital rate. Additionally, population-scale climate response curves reflect community dynamics, including competition between species, facilitative or mutualistic interactions, food web (consumer-resource) relationships, disturbance processes, source-sink dynamics, and community sorting (*e.g.*, priority effects).

Species Scale. At the scale of a species' geographic distribution, climate response curves reflect all the above processes. In addition, it is widely recognized that climatically suitable habitat may not be occupied because the species' rate of dispersal may prevent (limit) it from colonizing a given location (*dispersal limitation*). In fact, all these processes (plasticity, demography, competition and other interspecific interactions, disturbance processes, evolution, dispersal, *etc.*) operate at all scales all the time. Different sources of data, with different temporal and spatial

extent and resolution, offer more or less insight into direct cause-effect relationships and which processes are important influences on pattern at each scale.

Study species

Pinus edulis Engelm. (Colorado, common, or two-needle piñon) is a small-statured, slow-growing, stress-tolerant pine that can survive more than 500 years. It is endemic to the Colorado Plateau of the southwestern U.S. states of Arizona, Colorado, New Mexico, and Utah, where potential evapotranspiration exceeds precipitation in most months (8). Because it occurs across a wide range of elevation (1400-2700 m), *P. edulis* grows under a wide range of temperature conditions (mean annual temperature [MAT] of 4-17° C; Fig. S3). There is a gradient of monsoon moisture (in July and August, Fig. S11) increasing from north to south across *P. edulis*' distribution (8).

Tree-Ring Data

Tree-ring data were derived from increment cores sampled in the U.S. Forest Service Forest Inventory and Analysis (FIA) Program's spatial network of permanent sampling plots, during forest inventories between 1995 and 2013 (especially 1995-1997; (9, 10). Samples were processed to generate annually resolved time series at the University of Arizona Laboratory of Tree-Ring Research and at Utah State University, following standard dendrochronological protocols (9, 11): mounted on grooved boards, sanded to a fine polish, crossdated to assign a year of formation to each growth ring, and measured on a calibrated sliding stage micrometer. Year assignments were verified using COFECHA (12) before any analyses of the ring width time series. Start dates of the time series ranged from 1530 to 1983, but data analysis was limited to the period for which gridded climate data products are available (1895-1995).

Regression modeling of tree-ring width

We used a Bayesian hierarchical regression model to evaluate the predictions of Hypotheses 1 vs. 2 about patterns of variation in *P. edulis*' performance with variation in climate across space and time. This model predicted the log-transformed width of growth rings as a function of tree size and climate variables. Tree size (stem diameter at root collar, DRC) was included as a predictor because ring widths are known to change with tree size – radial growth increments are wide when a tree is small and become narrower as a tree becomes larger (13). Starting with the DRC measurement at the time that an increment core was sampled (available from the FIA database), DRC was back-calculated based on the tree-ring time series, generating an inferred DRC for every tree in every year. In addition to these fixed effects, we specified random tree effects – *i.e.*,

a modification of the model intercept specific to each tree – capturing heterogeneity among trees in average growth rate not explained by site-specific mean annual temperature (MAT) and mean annual precipitation (MAP) data.

Both spatially varying and spatio-temporally varying climate predictors were included in models of *P. edulis* growth, the first to capture how growth varies across spatial gradients of climate and the second to capture plastic responses to interannual climate variability (*i.e.*, reaction norms). Both types of climate predictors were created from time series of monthly, 4-km resolution climate data downloaded from the PRISM Climate Group (14) for the period 1895-2018. Climate normals, which vary strictly across space, were created by averaging monthly mean temperature and summing monthly precipitation of each year (January-December), then averaging across years to calculate mean annual temperature (MAT) and mean annual precipitation (MAP). To make time-varying climate predictors, the time series of monthly climate data were aggregated across a twelve-month time frame (previous September to current August) and four biologically relevant seasons: fall (September through October of the previous year), winter (previous November through the current year's March), spring (current year April through June) and monsoon (July through August). These four seasonal climate variables represent two wet seasons, one warm (monsoon) and one cold (winter), along with two warm, dry seasons (spring, fall; Fig. S11). Responses to time-varying climate were modeled as linear, which is traditional in dendrochronology (11, 13). While a few recent analyses of tree-ring data have shown nonlinearity in responses to climate (15, 16), and some reaction norms (*e.g.*, thermal response curves) are theoretically expected to peak between minimum and maximum climate values (7), field-observed values of performance vs. climate may be adequately predicted with a linear response across the historic, field-observed range of variability of climate, as described above, in "*Climate Responses across Scales*" (see Fig. S10B).

Though we had specific hypotheses to test (Fig. 1), it is important to verify that the model structure corresponding to those hypotheses adequately describes variation in *P. edulis* performance across space and time, *i.e.*, is not outcompeted by alternative models. We report here the fit to data of ten alternative Bayesian hierarchical regression models (Table S2), which included different combinations of climate predictors (normals, time-varying) and different methods of scaling during standardization (*i.e.*, centering and scaling of predictors to a mean of zero and standard deviation of one). Specifically, time-varying climate predictors were standardized using either global or local scaling. Global scaling compares temperature or precipitation at a given site each year to the global average for that variable across both space and time, whereas local scaling compares each year's climate to the local site average for that variable. Locally scaled variables thus reflect climate anomalies relative to average conditions at each site. The hypothesis under global scaling is that a temperature of 10° C and temperature variation of 1° C has the same effect on all trees throughout the geographic distribution, whereas

the hypothesis under local scaling is that a temperature of 10° C may be relatively cool at the warm edge of the distribution and relatively warm at the cool edge of the distribution, and that the effect of climate variability is best described relative to what trees are adapted to at a given location. Hence, the fit of data to models with globally vs. locally scaled climate predictors represents a secondary test comparing the hypotheses that climate responses are best described at the species scale (Hypothesis 1) vs. population or individual scale (Hypothesis 2).

The ten models are generally ordered from simpler to more complex. Model 1 tested the hypothesis that the climate normals MAP and MAT alone are sufficient to explain variation in *P. edulis* growth. Model 2 repeated Model 1 with the addition of tree size. Model 3 tested the hypothesis that time-varying climate, in addition to climate normals and tree size, explain growth variation, using globally scaled, 12-month cumulative precipitation and average temperature. Models 4-6 tested alternative seasonal time-varying climate predictors (both precipitation and temperature), which were globally scaled (Table S2). Models 7 and 8 test the hypothesis that the climate normals MAP and MAT do not significantly influence *P. edulis* growth (by removing them), with Model 7 using global scaling and Model 8 local scaling of the time-varying climate predictors. Model 9 tested the same seasonal climate predictors as Model 6, using local scaling for the time-varying predictors. Model 10 was unique in testing the use of both locally and globally scaled versions of the time-varying climate predictors of Model 6. All models included all two-way interactions between predictors, and all but Model 1 included the effect of tree size (Table S2).

Regression modeling was implemented using R, RStudio, and STAN (17), in the computational environment of VICE and the Discovery Environment of CyVerse (www.cyverse.org). Markov chain Monte Carlo simulations were run with 3 chains of 5000 iterations each, discarding the first 1000 iterations as warmup, resulting in 12,000 posterior samples. Convergence was assessed using visual inspection of traceplots and Gelman-Rubin diagnostics (18). Models were fit with a randomly selected 80% of the growth ring measurements and were validated with the remaining 20% of these held-out data using the root mean squared error (MSE) of model-predicted tree-ring width under a 5-fold cross-validation procedure. In addition, a full data fit using the approximate leave-one-out (elpd) information criterion (19–21); Fig. S9) was used to evaluate model performance. Model fit was also assessed visually using posterior predictive checks (18). The model fit statistics showed that seasonal time-varying climate variables predict *P. edulis*'s growth variability better than 12-month time-varying climate variables (Models 5 and higher fit better than Model 4), and that local scaling outperforms global scaling of the time-varying climate variables (Model 9 compared to Model 6, and Model 8 compared to Model 7; Fig. S9). Further, the inclusion of both climate normals and time-varying climate variables is supported (Model 9 fit the data better than Models 8 and 7; Fig. S9). Among the ten models fit to the ring-width data, two rose to the top in terms of low MSE and elpd: Models 9 and 10 (Fig. S9). We selected Model 9 as the preferred best-fit model, which included MAP and

MAT, four seasonal time-varying climate predictors - spring and fall temperatures and winter and monsoon precipitation - and all 2-way interactions between fixed effects.

The posterior predictive distribution diagnostics for Model 9 (pointwise posterior predictive credible intervals, probability integral transform overlay, and probability integral transform q-q plots; Fig. S12) illustrate a good fit to the bulk of the data but show some evidence of misfit for very small and very large tree-ring width observations. We plotted model residuals as a function of each of the time-varying climate predictors to check for systematic misfit that might result from modeling log-transformed ring widths as a linear response of interannual climate variation. The residuals showed no trend with respect to spring or fall temperature variation or monsoon precipitation variation among years, but there was some trend in the residuals with respect to variation in winter precipitation (blue trend lines, Fig. S13). There is a modest pattern of more extreme negative residuals at both the lowest and highest observed values of winter precipitation, indicating that the model tends to over-predict growth ring widths in the driest and wettest winters, respectively (Fig. S13B). Noticeable in all four panels of Fig. S13 are data points with strong negative residuals (the cloud of points below most of the rest of the residuals, in each panel) – these are cases where observed growth ring widths are much smaller than the predictions of the model. These are the year and tree combinations in which a growth ring was not produced, which we replaced with 0.001 mm (the smallest non-zero observation in our data), since the log of zero is undefined. Part of the trend in the residuals in Fig. S13B seems to arise from the association of the “missing ring” years with low values of winter precipitation. In other words, missing rings tend to be produced when winter precipitation is low. The trend of negative residuals at high values of winter precipitation suggests that there may be some leveling off (saturation) of the response of tree growth to the highest values of winter precipitation, as discussed above in “*Climate Responses across Scales*” (see Fig. S10A). Overall, this trend in residuals is modest and we considered linear responses to climate to be adequate to describe the variation in the data. A future improvement to modeling tree ring widths would be to use a Tobit or other mixture model to better capture the conditions that drive the formation of missing rings.

Because Model 9 performed well across predictive metrics and showed good evidence of fit from the posterior predictive diagnostic plots, the output of Model 9 was used for testing Hypotheses 1 vs. 2 and to create Fig. 2-3 and Fig. S4-S7. We note that across all ten models, the effects of climate were consistent in sign and magnitude, lending confidence in the robustness of these effects to alternative model structures.

Climate responses

All estimated fixed effects (including interactions) from Model 9 are shown in Fig. S4. In a soil moisture-limited species (*P. edulis*), we expected to see higher-than-average growth in both

cooler-than-average years and locations (Fig. 1D) because lower rates of evaporation with lower temperatures should weaken soil moisture-limitation of growth. Instead, the negative effect on *P. edulis'* growth of interannual variability in temperature ($\beta_{springtemp}$ = -0.0965, 95%CI = -0.1076 – -0.0857 and $\beta_{falltemp}$ = -0.0723, 95%CI = -0.826 – -0.0618) is contrasted by a positive effect of spatial variation in mean annual temperature (β_{MAT} = 0.2083, 95% CI = 0.1661 – 0.2506). Further, there is a significant positive interaction between the climate normals (fig. S4, $\beta_{MAT*MAP}$= 0.0438, 95% CI = 0.0097 – 0.0775), indicating that as mean annual temperature increases, the positive influence of mean annual precipitation (β_{MAP} = 0.2355, 95% CI = 0.1940 – 0.2771) on growth increases (and *vice versa*). Hence, growth rates of *P. edulis* are greatest at warmer-than-average sites, but especially those that are also wetter-than-average (blue lines, Fig. 2C-D). This may best be interpreted in terms of Liebig's law of the minimum. Among wetter-than-average sites, where soil moisture is less limiting, the influence of another limiting factor becomes evident: trees at cold but relatively wet sites are still unable to grow rapidly (blue lines, Fig. 2A-B), whereas those at warm but relatively wet sites can. We summarize *P. edulis*' observed climate-growth relationships in abstract form in Figure S8B, in contrast to the predicted climate-growth relationships in fig. S8A.

Finally, negative model-predicted responses to greater-than-average winter precipitation are seen at a very small number of cold, wet locations (*e.g.*, blue lines, Fig. 3A; Fig. S6C), which may represent high-elevation sites where a year of deep snowpack can limit the growing season and hence tree growth.

References

1. J. Franklin, *Mapping Species Distributions: Spatial Inference and Prediction* (Cambridge University Press, 2010).
2. A. T. Peterson, *et al.*, *Ecological Niches and Geographic Distributions (MPB-49)* (Princeton University Press, 2011).
3. J. Elith, J. R. Leathwick, Species Distribution Models: Ecological Explanation and Prediction Across Space and Time. *Annu. Rev. Ecol. Evol. Syst.* **40**, 677–697 (2009).
4. S. Pironon, *et al.*, Geographic variation in genetic and demographic performance: new insights from an old biogeographical paradigm. *Biol. Rev.* **92**, 1877–1909 (2017).
5. M. Bontrager, *et al.*, Adaptation across geographic ranges is consistent with strong selection in marginal climates and legacies of range expansion. *Evolution* **75**, 1316–1333 (2021).
6. S. Pironon, *et al.*, The 'Hutchinsonian niche' as an assemblage of demographic niches: implications for species geographic ranges. *Ecography* **41**, 1103–1113 (2018).
7. M. J. Angilletta Jr., Thermal Adaptation: A Theoretical and Empirical Synthesis. *Therm. Adapt. Theor. Empir. Synth.* 1–302 (2009). https://doi.org/10.1093/acprof:oso/9780198570875.001.1.
8. R. F. Miller, *et al.*, The ecology, history, ecohydrology, and management of pinyon and juniper woodlands in the Great Basin and Northern Colorado Plateau of the western United States. *Gen Tech Rep RMRS-GTR-403 Fort Collins CO US Dep. Agric. For. Serv. Rocky Mt. Res. Stn. 284 P* **403** (2019).
9. R. J. DeRose, J. D. Shaw, J. N. Long, Building the Forest Inventory and Analysis Tree-Ring Data Set. *J. For.* **115**, 283–291 (2017).
10. W. A. Bechtold, P. L. Patterson, Editors, The enhanced forest inventory and analysis program - national sampling design and estimation procedures. *Gen Tech Rep SRS-80 Asheville NC US Dep. Agric. For. Serv. South. Res. Stn. 85 P* **080** (2005).
11. J. Speer, *Fundamentals of Tree Ring Research* (2010).
12. R. L. Holmes, Computer-Assisted Quality Control in Tree-Ring Dating and Measurement. (1983).
13. H. C. Fritts, *Tree Rings and Climate* (Academic Press, 1976).
14. PRISM Climate Group, Oregon State University. (2004). Available at: https://prism.oregonstate.edu/.
15. M. P. Dannenberg, E. K. Wise, W. K. Smith, Reduced tree growth in the semiarid United States due to asymmetric responses to intensifying precipitation extremes. *Sci. Adv.* **5**, eaaw0667 (2019).
16. J. Gantois, New tree-level temperature response curves document sensitivity of tree growth to high temperatures across a US-wide climatic gradient. *Glob. Change Biol.* **28**, 6002–6020 (2022).
17. Stan Development Team, *Stan User's Guide*, 2.32.
18. A. Gelman, D. B. Rubin, Inference from Iterative Simulation Using Multiple Sequences. *Stat. Sci.* **7**, 457–472 (1992).
19. A. Vehtari, A. Gelman, J. Gabry, Practical Bayesian model evaluation using leave-one-out cross-validation and WAIC. *Stat. Comput.* **27**, 1413–1432 (2017).
20. A. Gelman, X.-L. Meng, H. Stern, POSTERIOR PREDICTIVE ASSESSMENT OF MODEL FITNESS VIA REALIZED DISCREPANCIES. *Stat. Sin.* **6**, 733–760 (1996).
21. J. Gabry, D. Simpson, A. Vehtari, M. Betancourt, A. Gelman, Visualization in Bayesian workflow. *J. R. Stat. Soc. Ser. A Stat. Soc.* **182**, 389–402 (2019).

22. E. L. Little, *Atlas of United States trees* (U.S. Dept. of Agriculture, Forest Service, 1971).
23. T. Dallas, R. R. Decker, A. Hastings, Species are not most abundant in the centre of their geographic range or climatic niche. *Ecol. Lett.* **20**, 1526–1533 (2017).
24. T. A. Dallas, A. Hastings, Habitat suitability estimated by niche models is largely unrelated to species abundance. *Glob. Ecol. Biogeogr.* **27**, 1448–1456 (2018).
25. B. J. McGill, Trees are rarely most abundant where they grow best. *J. Plant Ecol.* **5**, 46–51 (2012).
26. G. Midolo, C. Wellstein, S. Faurby, Individual fitness is decoupled from coarse-scale probability of occurrence in North American trees. *Ecography* **44**, 789–801 (2021).
27. M. F. Oldfather, D. Ackerly, Linking demography and microclimate across the range of an alpine plant in (ESA, 2017).
28. T. Bohner, J. Diez, Extensive mismatches between species distributions and performance and their relationship to functional traits. *Ecol. Lett.* **23**, 33–44 (2019).
29. K. C. Baer, J. L. Maron, Ecological niche models display nonlinear relationships with abundance and demographic performance across the latitudinal distribution of Astragalus utahensis (Fabaceae). *Ecol. Evol.* **10**, 8251–8264 (2020).
30. M. Bernal-Escobar, D. Zuleta, K. J. Feeley, Changes in the climate suitability and growth rates of trees in eastern North America. *Ecography* **2022**, e06298 (2022).
31. M. L. DeMarche, *et al.*, Latitudinal gradients in population growth do not reflect demographic responses to climate. *Ecol. Appl.* **31**, e2242 (2021).
32. J. M. Diez, I. Giladi, R. Warren, H. R. Pulliam, Probabilistic and spatially variable niches inferred from demography. *J. Ecol.* **102**, 544–554 (2014).
33. M. F. Oldfather, M. J. Koontz, D. F. Doak, D. D. Ackerly, Range dynamics mediated by compensatory life stage responses to experimental climate manipulations. *Ecol. Lett.* **24**, 772–780 (2021).
34. J. Pagel, *et al.*, Mismatches between demographic niches and geographic distributions are strongest in poorly dispersed and highly persistent plant species. *Proc. Natl. Acad. Sci.* **117**, 3663–3669 (2020).
35. W. Thuiller, *et al.*, Does probability of occurrence relate to population dynamics? *Ecography* **37**, 1155–1166 (2014).
36. S. M. Amburgey, *et al.*, Range position and climate sensitivity: The structure of among-population demographic responses to climatic variation. *Glob. Change Biol.* **24**, 439–454 (2018).
37. U. Bradter, *et al.*, Decomposing the spatial and temporal effects of climate on bird populations in northern European mountains. *Glob. Change Biol.* **28**, 6209–6227 (2022).
38. P. Gaüzère, V. Devictor, Mismatches between birds' spatial and temporal dynamics reflect their delayed response to global changes. *Oikos* **130**, 1284–1296 (2021).
39. F. La Sorte, T. Lee, H. Wilman, W. Jetz, Disparities between observed and predicted impacts of climate change on winter bird assemblages. *Proc. Biol. Sci.* **276**, 3167–74 (2009).

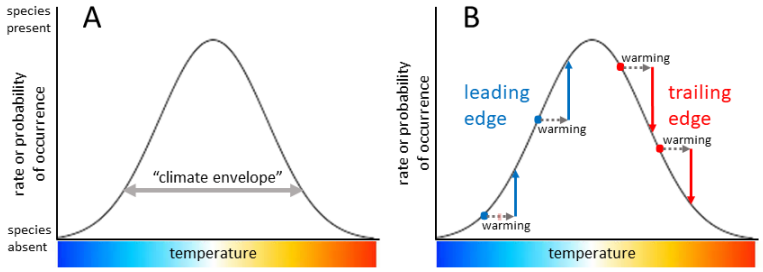

374

375 **Fig. S1.** Conceptual illustration of (A) a species' climate envelope, inferred from presence-
376 absence or presence-only data, with respect to a single dimension of climate (a temperature
377 variable). This species-level climate response is then used to project (B) the effect of climate
378 change (warming) on the species' rate or probability of occurrence.

379

380

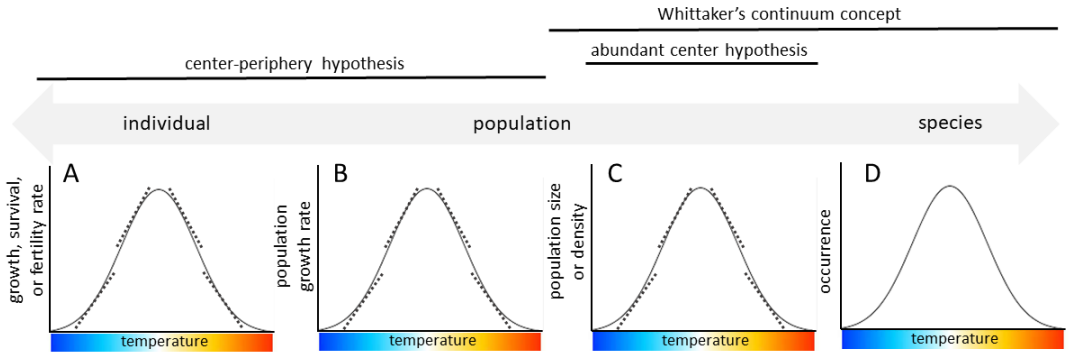

Fig. S2. Responses to temperature variability at the (A) individual, (B-C) population, and (D) species scale. The use of climate envelope models to forecast change in species' distributions effectively assumes that climate responses are the same across scales, as illustrated here. Solid lines indicate a scenario in which individual- and population-scale climate responses are equal in breadth to the species-scale response; dashed lines indicate the case where individual- and population-scale climate tolerances are narrower than species-scale climate tolerances, but they match in local slope (the sign of the response). Ecological theories that support the assumption of scale-invariant climate responses are placed above the biological scale axis.

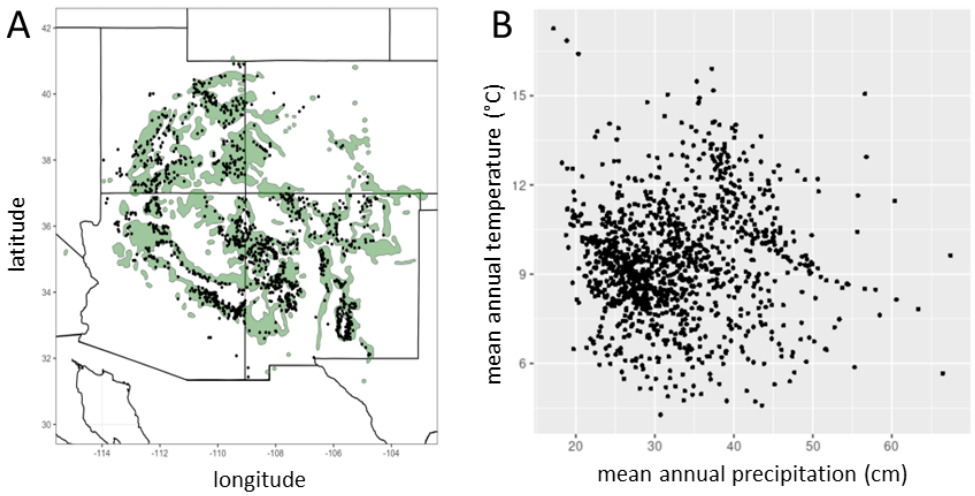

Fig. S3. Location in (A) geographic and (B) climate space of the 977 U. S. Forest Service Forest Inventory and Analysis (FIA) plots in the U. S. states of Arizona, New Mexico, Colorado, and Utah where *Pinus edulis* increment cores were collected. Green in panel A is the geographic distribution of *Pinus edulis*, as defined in the atlas of U. S. trees (22).

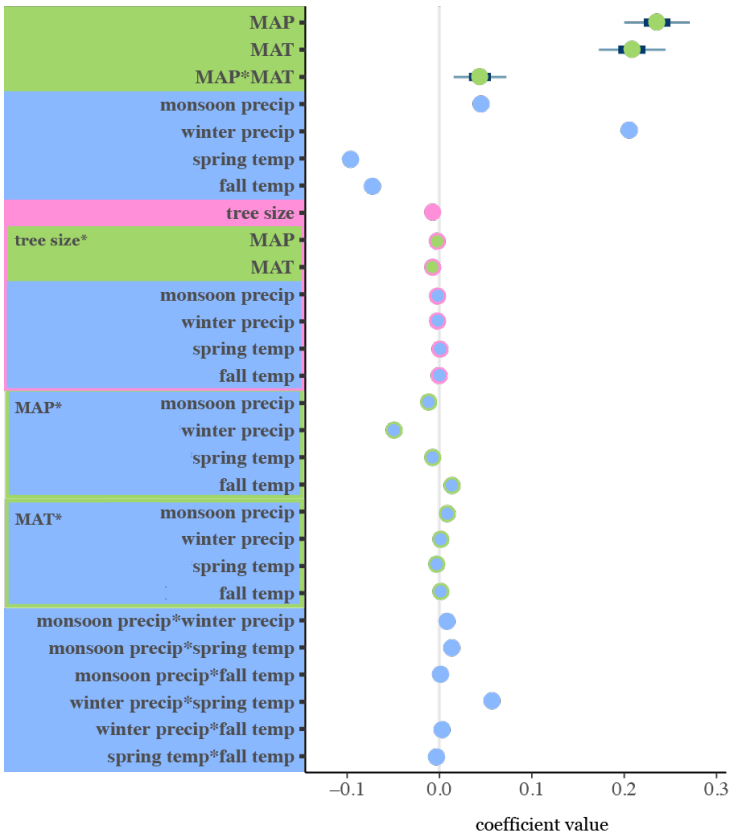

Fig. S4. Estimates of effects from a multiple regression model of *P. edulis* growth (model 9 in Table S2). Each dot-whisker shows the Bayesian posterior distribution of a model parameter (posterior mean +/- 95% central density). Predictors were centered and scaled, with the exception of tree size. Main effects are color-coded into three groups: climate normals (green), time-varying climate variables (blue), and tree size (pink). Two-way interaction effects are color-coded accordingly both in the y-axis label and the dot-whisker.

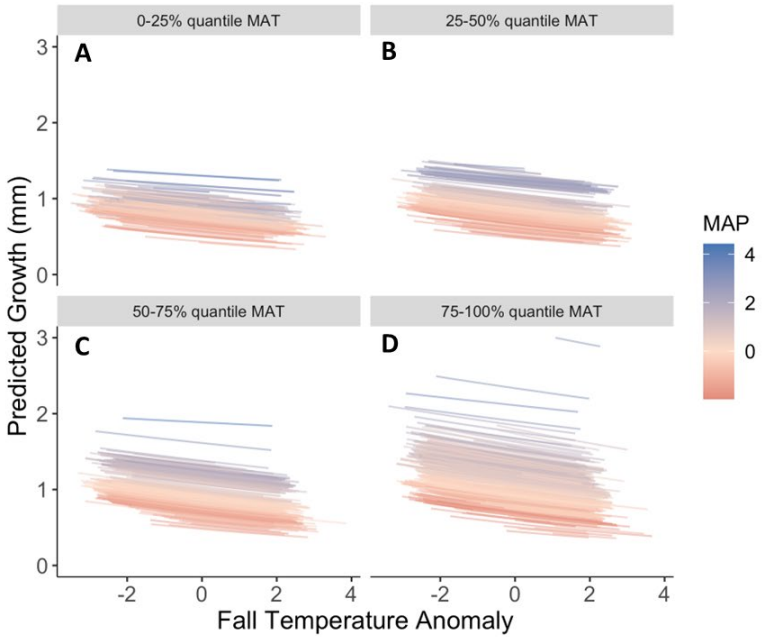

Fig. S5. Model-predicted responses to fall temperature variability of all 1,558 common pinon trees in the dataset, at locations that vary from cool to warm (quantiles of mean annual temperature [MAT], averaged over the period 1895-2018), with each response colored by the mean annual precipitation (MAP) at that location, from dry (red) to wet (blue). Fall temperature is the average of monthly average temperatures September-October of the previous calendar year, locally scaled, *i.e.*, anomalies relative to site-specific average fall temperature. Responses are plotted for a constant tree size of 20 cm.

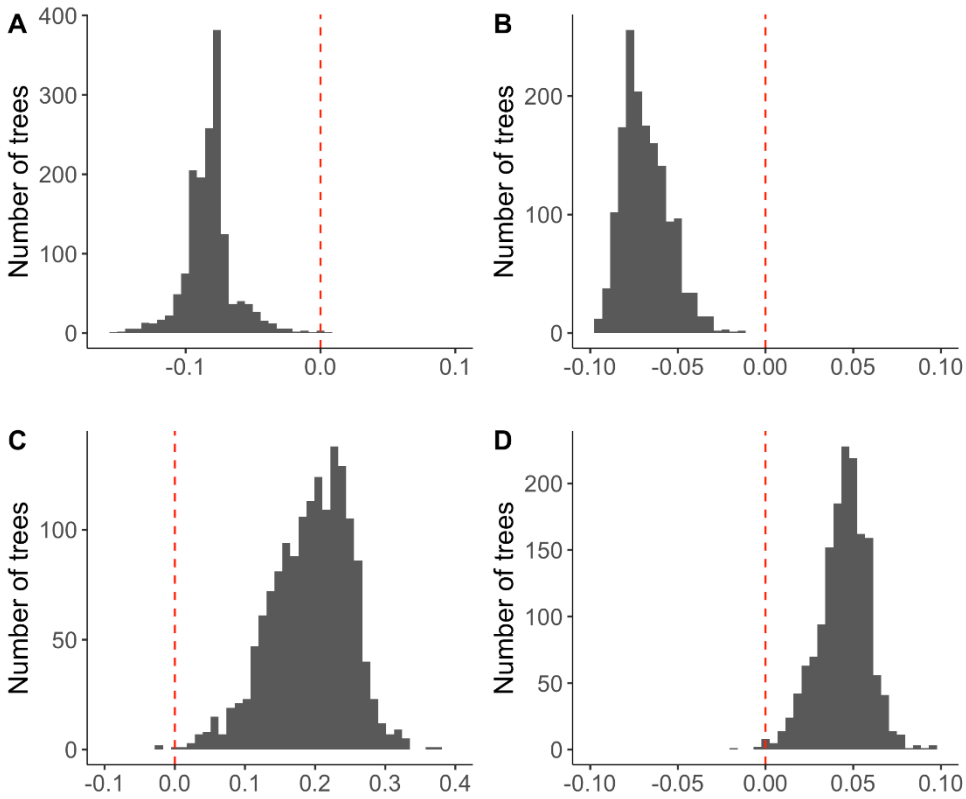

Fig. S6. Histograms of the sensitivity of the growth of 1,558 *Pinus edulis* trees to four time-varying climate predictors: (A) spring and (B) previous fall temperature, and (C) winter and (D) monsoon precipitation. These sensitivities correspond to the slopes of the lines in Fig. 2, Fig. S5, Fig. 3, and Fig. S7, respectively, although here the slope is change in *log-transformed* growth-ring width in response to variation in each climate predictor.

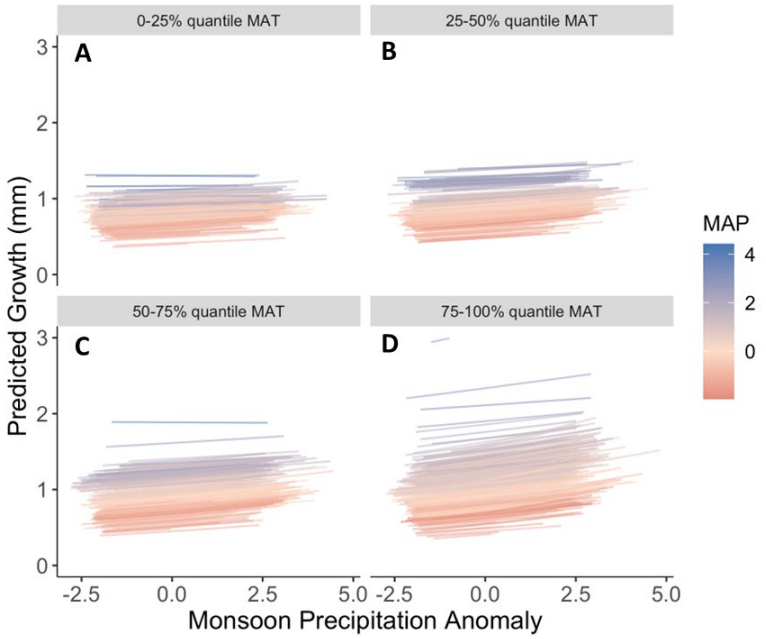

Fig. S7. Model-predicted responses to monsoon precipitation variability of all 1,558 common pinon trees in the dataset, at locations that vary from cool to warm (quantiles of mean annual temperature [MAT], averaged over the period 1895-2018), with each response colored by the mean annual precipitation (MAP) at that location, from dry (red) to wet (blue). Monsoon precipitation is the sum of precipitation in July and August of the current calendar year, locally scaled, *i.e.*, anomalies relative to site-specific average monsoon precipitation. Responses are plotted for a constant tree size of 20 cm.

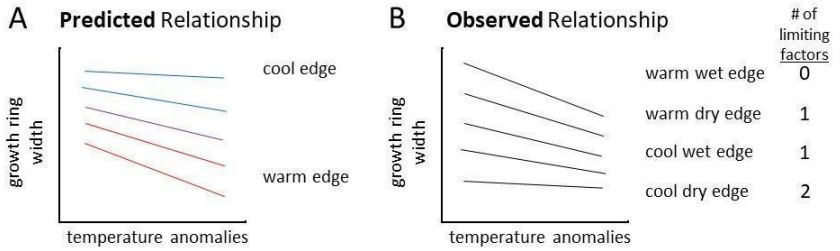

Fig. S8. Predicted vs. observed relationships between tree growth and interannual temperature variability across the distribution of a (A) hypothetical soil moisture-limited species (as in Fig. 1E), and (B) *Pinus edulis*.

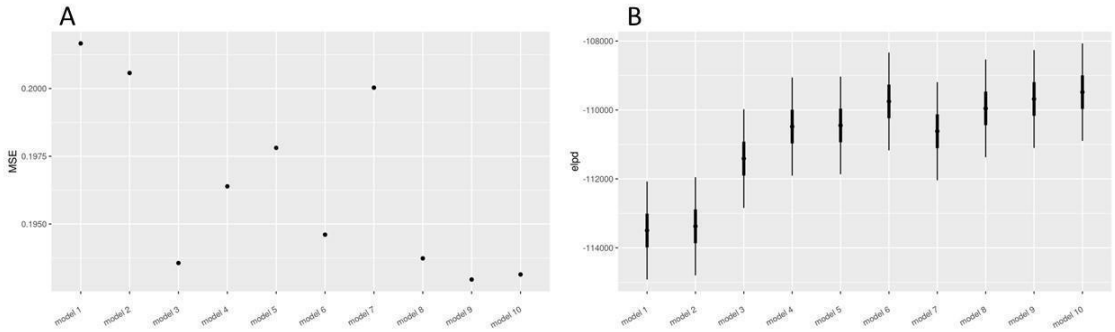

Fig. S9. Fit of ten alternative regression models to *Pinus edulis* tree-ring width data, with respect to (A) root mean squared error (MSE) and (B) approximate leave-one-out information criterion (elpd). All ten models are detailed in Table S2.

443

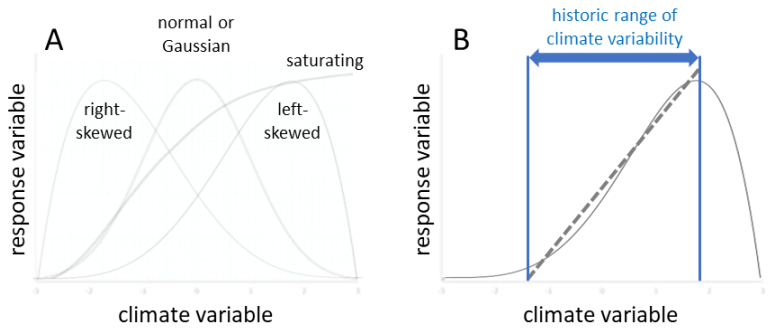

444

445 **Fig. S10.** Climate responses (A) may take a variety of shapes, from symmetric to skewed to
446 saturating. (B) A skewed response may be fit to field-collected data with a line, *i.e.*, across the
447 range of climate variability to which an organism is regularly exposed and therefore adapted.

448

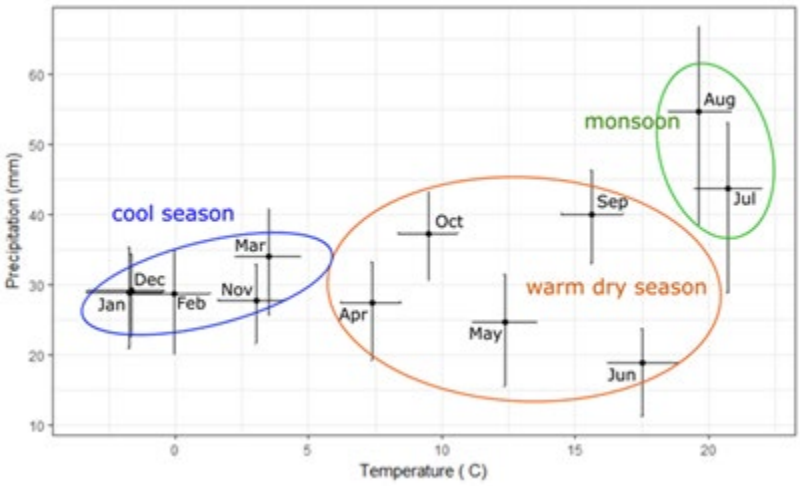

449

450 **Fig. S11.** Average monthly temperature and precipitation at U. S. Forest Service Forest Inventory
451 and Analysis plot locations where *Pinus edulis* is present, based on PRISM 4-km resolution
452 climate data.

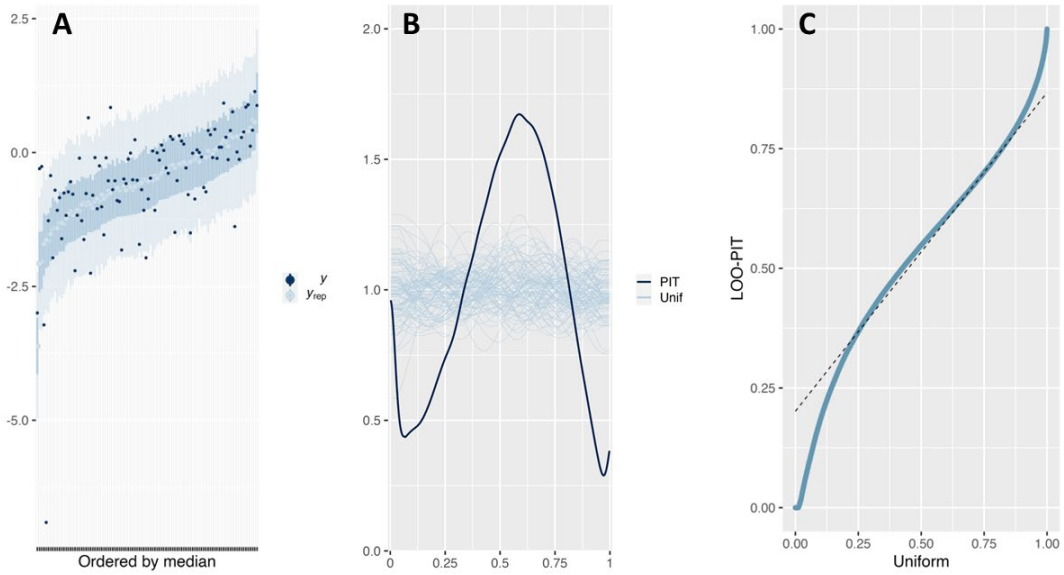

Fig. S12. Posterior predictive diagnostics for Model 9. (A) The 50% and 90% posterior predictive intervals for a subset of log tree-ring widths, ordered by posterior predictive mean (y_{exp}). Dark points are the observed log ring widths (y), which mostly fall within the 50% or 90% posterior predictive intervals. (B) Smoothed density of posterior predictive samples of log ring width in light blue and a smoothed density of observed log ring widths in dark blue. (C) Leave-one-out quartile-quartile plot of posterior predictive mean vs. observed log ring width.

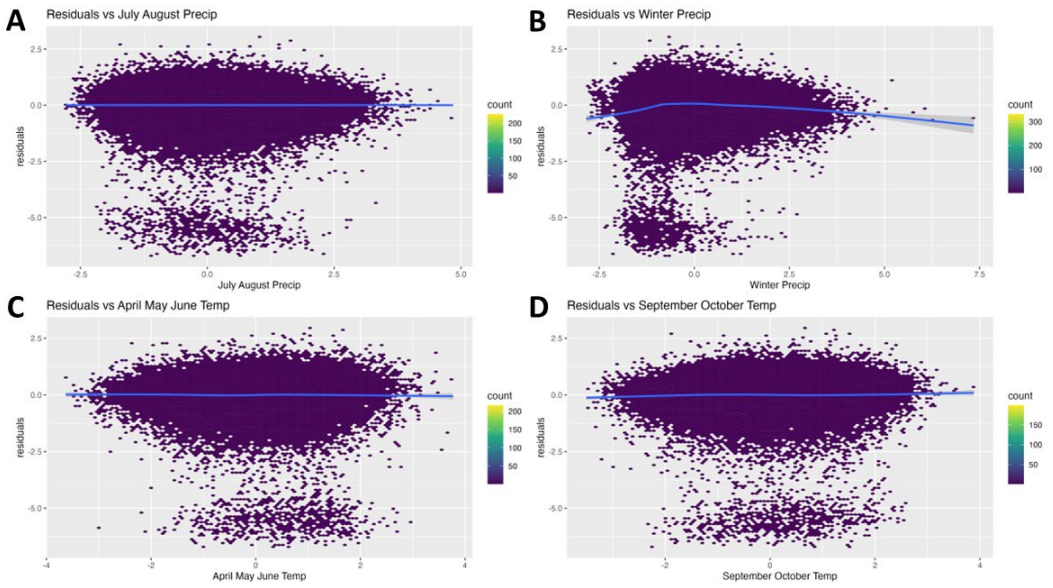

Fig. S13. Residuals of model 9 plotted against the four time-varying climate predictors: (A) monsoon precipitation, (B) winter precipitation, (C) spring temperature, and (D) previous fall temperature. A generalized additive model fit to the residuals in each panel, shown with a blue line, evaluates trend in model residuals.

Table S1. Corroborating evidence of scale-dependent climate responses: mismatches between individual-level vital rates (*e.g.*, growth, survival, fertility, recruitment), population-level growth rate or abundance, and species-level occurrence, probability of occurrence, or climatic suitability derived from occurrence data in the recent literature. The citation is followed by a description of the scope of the data (organism, spatial and temporal replication, location), then the type of data analyzed, or variables estimated from data, then a description of the mismatch, reproduced from the title or abstract of the citation or summarized succinctly. Where possible, we list (in parentheses) whether the study considered spatial vs. temporal variation in the individual- and population-level variables. Species-level variables (*e.g.*, climatic suitability) vary only across space (with some exceptions). Citations are grouped into four categories: those addressing 1) the abundant center hypothesis or 2) center-periphery hypothesis, those 3) analyzing individual-level performance variation across space and time and fitting a demographic model to estimate population-level growth rate, and 4) those that explicitly consider distinct variation across space vs. time. This list of citations is surely incomplete, and alternative placement of a given paper into a different category is possible.

482

Citation	Study organism, sample size, (location)	Individual	population	species	Description of mismatch
Abundant center hypothesis					
Dallas et al. 2017 (23)	1109 bird species, 81 mammal species, 63 fish species, 166 tree species (the Americas)		abundance (spatial)	geographic distribution, climatic niche	species are not most abundant in the center of their geographic distribution or climatic niche
Dallas & Hastings 2018 (24)	246 mammal species, 148 tree species (USA)		abundance (spatial)	climatic suitability	climatic suitability estimated by niche models is largely unrelated to species abundance
Center-Periphery Hypothesis					
McGill 2012 (25)	15 tree species (eastern North America)	growth (spatial variation in 46-yr average rate)	abundance (spatial)		trees are rarely most abundant where they grow best
Midolo et al. 2021 (26)	66 tree species (North America)	growth (spatial variation)		probability of occurrence	individual fitness is decoupled from coarse-scale probability of occurrence
Oldfather & Ackerly 2017 (27)	16 populations of a perennial plant, years 2014-2017 (one mountain range, California, USA)	growth, survival, and recruitment (spatial and temporal variation)	population growth rate (spatial and temporal variation)		vital rates and population growth rate do not decline from the center to the edges of the species' elevational range
Pironon et al. 2017 (4)	review of 248 empirical studies (all taxa)	genetic variation, growth, survival, recruitment	genetic variation, abundance, population growth rate	geographic distribution, climatic niche	demographic vital rates, population size, and population growth rate follow center-periphery expectations in only 20-30% of studies
Bohner & Diez 2019 (28)	59 tree species (western USA)	growth, survival, and recruitment (spatial variation in 10-yr average rates)	population density (spatial)	probability of occurrence	extensive mismatches between peak probability of occurrence and peak population density or individual-level demographic rates
Demographic (vital) rates					
Baer and Maron 2020 (29)	11 populations of a perennial plant, years 2013-2016	growth, survival, fecundity,	abundance, population growth rate	climatic suitability	positive (but nonlinear) relationship between a) climatic suitability vs. b) abundance and demographic performance

	(Utah and Idaho, USA)	germination (spatial and temporal variation)	(spatial and temporal variation)		(latitudinal gradient, range center to range edge)
Bernal-Escobar et al. 2022 (30)	37 species of trees, 558 populations (eastern North America)	growth (spatial and temporal variation, moving window 30-year average growth rate)		climatic suitability (spatial and temporal variation, moving window 30-year probability of occurrence)	changes in individual growth rate were negatively correlated with changes in climatic suitability
DeMarche et al. 2021 (31)	3 species of perennial plants, 5-7 populations per species, years 2015-2018 (Oregon and Washington, USA)	growth, survival, fecundity, recruitment (spatial and temporal variation treated as equivalent)	population growth rate (spatial and temporal variation)		latitudinal gradients in performance are not predictive of either local or species-wide responses to climate; population growth rate is lower at cool and wetter locations, but is lower in warmer and drier years; opposite response across space vs. time (latitudinal gradient from center to northern edge of their distributions)
Diez et al. 2014 (32)	perennial plant, 6 populations (one watershed, eastern USA)	growth, survival, and recruitment (spatial and temporal variation treated as equivalent)	abundance, population growth rate (spatial variation)	occurrence	demographic suitability did not predict occurrence, but demographic suitability and abundance were positively correlated
Oldfather et al. 2021 (33)	perennial plant, 9 populations (elevation gradient, one mountain range, California, USA)	growth, survival, recruitment (spatial and temporal)	population growth rate (spatial and temporal)		lack of concordance between spatial patterns of population growth rate with climate gradients and the response of population growth rate to experimental climate manipulations; cool-edge populations did not respond positively to warming
Pagel et al. 2020 (34)	26 perennial plant species (South Africa)	3,617 records of survival, fecundity, and recruitment	population growth rate (spatial)	occurrence	mismatches between demographic suitability (population growth rate) and observed geographic distributions
Pironon et al. 2018 (6)	2 short-lived herbaceous plants; 11 and 20 populations per species (Europe,	growth, survival, fecundity, recruitment (spatial and	population growth rate (spatial and temporal)	occurrence	occurrence and performance niches cannot be assumed to be the same

	California, USA)	temporal)			
Thuiller et al. 2014 (35)	108 tree species (western USA, Quebec, France, Switzerland)	basal area (spatial and temporal)	population growth rate, carrying capacity, and abundance	probability of occurrence	population growth rate was negatively correlated with probability of occurrence, while carrying capacity and abundance were positively correlated with probability of occurrence
Space vs. Time not equivalent					
Amburgey et al. 2018 (36)	one species of frog, 746 populations at 27 locations, 3-22 years (North America)	fertility (spatial and temporal)	population growth rate (spatial and temporal)	climatic distribution	sensitivity of population growth rate to interannual climate variability changes in sign across the climatic distribution for some climate variables and not others
Bradter et al. 2022 (37)	39 bird species, 1756 survey routes, years 1996-2018 (Fennoscandia)		abundance (spatial and temporal)		the assumption of equivalent species' response to spatial and temporal variation in climate was seldom met
Gaüzère & Devictor 2021 (38)	124 bird species, 2133 sites, years 2001-2012 (France)		abundance (spatial and temporal)		quantified and mapped differences between spatial vs. temporal variation in abundance
La Sorte et al. 2009 (39)	227 bird species, 404 locations, 26 years (North America)		body mass (spatial and temporal)	occupancy (spatial and temporal)	trends of species richness, body mass, and occupancy through time differed significantly from spatially derived predictions, questioning space-for-time substitution

Table S2. Ten regression models predicting growth ring width variation of *Pinus edulis* as a function of tree size and climate variables. A numerical label and all main effects are listed for each model, as well as the type of scaling used for time-varying predictors (G for global scaling or L for local scaling). Seasons were defined as monsoon (m; Jul-Aug), winter (w; Nov-Mar), spring (s; Apr-Jun), and fall (f; Sep-Oct). Values of the model fit statistics root mean squared error (MSE) and leave-one-out (elpd) validation are shown in Fig. S9.

Model	Tree Size	Climate Normals	Time-varying Climate	Scaling
1		✓		
2	✓	✓		
3	✓	✓	12-month precip and temp	G
4	✓	✓	12-month temp, mw precip	G
5	✓	✓	mw precip, mw temp	G
6	✓	✓	mw precip, sf temp	G
7	✓		mw precip, sf temp	G
8	✓		mw precip, sf temp	L
9	✓	✓	mw precip, sf temp	L
10	✓	✓	mw precip, sf temp	G, L

Table S3. Model-fit statistics (deviance and AIC) for generalized additive models (GAMs) of *Pinus edulis*' occurrence in the U.S. Forest Inventory and Analysis plots of Arizona, Colorado, New Mexico, and Utah as a function of the climate conditions at plot locations (variables listed). GAMs were fit with five, four, and three knots (k).

Climate Variable	Deviance			AIC		
	k=5	k=4	k=3	k=5	k=4	k=3
Mean Annual Temperature	252.85	254.76	254.47	288.96	289.32	287.7
Mean Annual Precipitation	294.76	296.05	299.84	331.09	331.67	334.4
Monsoon Precipitation	289.94	302.46	302.98	327.88	337.39	337.68
Winter Precipitation	299.73	302.46	302.98	336.14	337.39	337.68
Fall Temperature	257.7	258.14	257.85	293.28	292.83	291.21
Spring Temperature	257.54	258.02	257.85	292.65	292.21	290.63